JOURNAL OF APPLIED GEOSPATIAL INFORMATION

Vol 5 No 1 2021

http://jurnal.polibatam.ac.id/index.php/JAGI
ISSN Online: 2579-3608

Development of $K_d(490)$ Algorithm Using Medium Spatial Resolution Landsat 8 Oli Arround Shallow Waters In Panggang Island

Budhi Agung Prasetyo [1,2]*, Wikanti Asriningrum [3], Vincentius Paulus Siregar [4]

* Corresponding author email: budhi.prasetyo@sll.itera.ac.id

[1] Marine Environmental Science Study Program, Institut Teknologi Sumatera, Jl. Terusan Ryacudu, Way Huwi, Kec. Jati Agung, Kabupaten Lampung Selatan, Lampung 35365 Indonesia
[2] Pusat Riset dan Inovasi Sains dan Informasi Geospasial, Institut Teknologi Sumatera, Jl. Terusan Ryacudu, Way Huwi, Kec. Jati Agung, Kabupaten Lampung Selatan, Lampung 35365 Indonesia
[3] Remote Sensing Applications Center, National Institute of Aeronautics and Space of Indonesia (LAPAN), Jl. Kalisari No.8, RT.11/RW.1, Pekayon, Pasar Rebo, East Jakarta City, Jakarta 13710 Indonesia
[4] Department of Marine Science and Technology, Faculty of Fisheries and Marine Science, IPB University, Jl. Agatis, Babakan, Kec. Dramaga, Kota Bogor, Jawa Barat 16128 Indonesia

Received: November 03, 2020
Accepted: January 16, 2021
Published: March 16, 2021

Abstract

The state of water quality around Panggang Island, Seribu Islands, in recent decades, experienced degradation caused by human activities. The parameter of the diffuse attenuation coefficient (K_d) is an important optical property-related attenuation of light in the water column and its brightness. Landsat 8 data has the potential to map the value of $K_d(490)$ in regional waters in Indonesia. Landsat 8 data could provide solutions to spatial data availability of $K_d(490)$ values in addition to Ocean Color data. This research aimed to develop an empirical algorithm of Landsat 8 data to derive $K_d(490)$ value, that can be used as tools for monitoring water quality optically on a regional scale, which could not be done by Ocean Color data that has spatial resolution limitation. The in-situ measurement of radiometric data was done using the TriOS-RAMSES hyperspectral spectroradiometer with a range of 320 – 890 nm and a spectral sampling of 3.3 nm shallow-waters around Panggang Island. The development of the $K_d(490)$ algorithm was done by simulation on the ratio of Green, and Near-infrared band has great determination values with $K_d(490)$ empirically. That empirical algorithm can be applied on Landsat 8 data to derive its values. It is also noted that the shallow-waters around Panggang Island, dominant affected by absorption of chlorophyll-a rather than scattering by suspended solids.

Keywords: Diffuse Attenuation Coefficient, $K_d(490)$, Landsat 8, Ocean Color, Algorithm

1. Introduction

In recent decades, the state of Seribu Island had been experienced degradation caused by human activities, such as fishery and recreational activities. Had been known that water quality in the waters around Seribu Island decreases due to an increase in human activities from the Jakarta Bay and shipping activities from Jakarta Bay to Seribu Island. One of the water quality that has been changed over time was water transparency. Parameters of water transparency can be monitor by approaching of remote sensing technology, such as the diffuse attenuation coefficient. The study of diffuse attenuation coefficients to determine the degree of water transparency based on the light attenuated into the water column has generally been done by the Ocean Color research community around the world (IOCCG 2000; IOCCG 2006). In Indonesia, the development of remote sensing technology for ocean color monitoring (Ocean Color) is commonly done. Ocean Color data has wide usage in Indonesia because of geographical conditions in Indonesia, consisting of hundreds of small islands that are widespread. In addition to being used for monitoring on extensive coverage area, Ocean Color data is also being used to extract information at small geographic coverage in an area, such as the application of the change in diffuse attenuation coefficient ($K_d(490)$) over Seribu Island, DKI Jakarta, Indonesia.

Diffuse attenuation coefficient, $K_d(\lambda)$ from downwelling irradiance, $E_d(\lambda)$, is one of seawater apparent optical properties that related to process of solar light penetrated through water column and availability of the aquatic system; also $K_d(\lambda)$ specifically at 490 nm or $K_d(490)$ is considered as proxy or limits to classified water cases (Jerlov 1976; Salama and Verhoef 2015; Wang et al. 2009). $K_d(\lambda)$ is one of the important parameters of seawater, which provides information on the availability of light in water column, and the level of light attenuated trough water column (Lee *et al.* 2005; Kirk 2011; Prasetyo *et al.* 2017).

One of the most popular marine remote sensing sensors commonly used to monitor or derived information about seawater or its column in Indonesia was MODIS-Aqua. MODIS-Aqua has a relatively large of spatial resolution, covering 250 m for Band 1 and 2, 500 m for Band 3 through 7, and 1 km for bands 8 to 36. The advantages of MODIS-Aqua sensors is large and wide area of coverage and has good of temporal data, so the researcher could monitor the wide area and in a daily basis, even in near-realtime (Hendiarti et al., 2006). MODIS-Aqua for usages of water transparency monitoring based on diffuse attenuation coefficient at 490 nm, $K_d(490)$, for areas with local coverage have disadvantages, i.e the spatial resolution was too broad, so the information that retrieved becomes less or not enough to study the patterns of $K_d(490)$ over small area such as in shallow-waters around Panggang Island.

The existence of the Landsat 8 Operational Land Imager (OLI) imagery data provides a potential for mapping and calculating the value of $K_d(490)$ over a small area in Indonesia waters, one of them in the waters around the Panggang Island of Seribu Island, DKI Jakarta. Landsat 8 OLI carrying sensors with a medium spatial resolution with a 30 m and has a wide area of the swath, Landsat 8 OLI data suitable for use as an input to monitor the water quality such as the value of $K_d(490)$ (Lymburner *et al.* 2016; Pahlevan and Schott 2013; Zheng *et al.* 2016). Based on the results of the previous research that's been done on the monitoring of water quality parameters over Indonesia sea by using Landsat 8 OLI, such as mapping of total suspended solids (TSS) and the water clarity in the oceanic waters and coastal waters has been done successfully (Parwati and Purwanto 2017; Arief 2017). Also, the previous research about the retrieval of $K_d(490)$ values based on Landsat 8 OLI data has been done successfully over inland turbid waters on Dongting Lake, China (Zheng et al., 2016). That previous research gave us opportunities for the utilization of Landsat 8 OLI imagery data that can be used as inputs for monitoring $K_d(490)$ over a small area in Seribu Island, DKI Jakarta, Indonesia.

The purposes of this research is to develop an algorithm of Landsat 8 OLI to derive $K_d(490)$ data in a regional scale that cannot be filled by using Ocean Color data because its limitation on spatial resolution, and to find out about the variability and patterns of the attenuation coefficient value in the waters around Panggang Island lagoon and Karang Lebar lagoon on Seribu Island, DKI Jakarta based on the $K_d(490)$ algorithm of Landsat 8 OLI.

2. Methods

2.1 Study Area

The field measurement was conducted on shallow waters around Panggang Island lagoon and Karang Lebar lagoon in Seribu Island, DKI Jakarta, Indonesia. Geographically the location of the research lies in the longitude 5º43'00" – 5º46'00" and in the latitude 106º33'30" – 106º37'30". Point of field measurement determined using line transect methods. Field measurement of optical properties was conducted in April 2016. There is six line transect which determined using stratified random sampling methods with the assumption that shallow waters around the lagoonal area has several groups of depth level, on the middle, on the edges and on the outside of lagoon (Figure1).

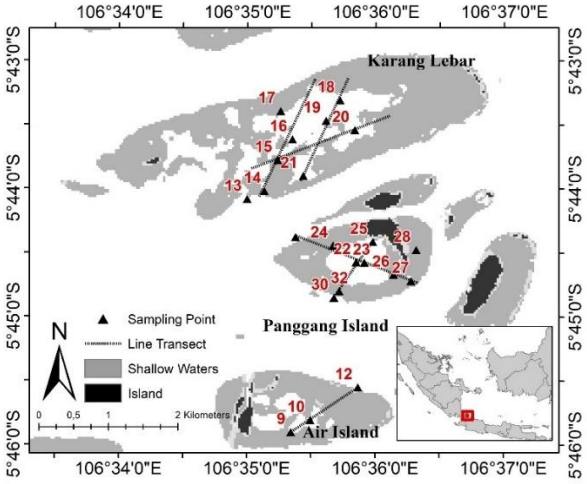

Fig. 1. Research locations

2.2 Data collection

This research is a further research from previous research that was done by Prasetyo *et al.* (2017) where the measurement is carried around of Panggang Island lagoon and Karang Lebar lagoon that was performed in April 2016. The data were used in this research were water quality parameters consisting of chlorophyll-*a*, suspended solids and radiometric data from an in-situ measurement. Also, we used the selected Landsat 8 OLI data to derive $K_d(490)$ values by using the new developed algorithm. The data collection procedure will be described as follows.

2.2.1 Water characteristic measurement

The measurement of water characteristics was conducted on our research location are water depth were done by using sounder gun, water transparency was done by using Secchi-disc, and also water sample was taken from water column (range 1-20 m) using Van-Dorn water sampler to be analyzed in the laboratory. The laboratory analysis was carried out to determine the concentration of chlorophyll-*a* and total suspended solid (TSS). The purposes of analyzing chlorophyll-a and TSS concentration to assess the influences of $K_d(\lambda)$ values to absorption and scattering of light in the water column (Prasetyo et al. 2017; Prasetyo et al. 2018).

2.2.2 Landsat 8 OLI imagery data acquisition

Monitoring on a temporal basis was conducted to study patterns of $K_d(490)$ values over time. The selected temporal time that we are using was at 2015, 2016, and 2017 with the location Path/Row 122/64. The data that acquired at 2016 was in near time with in-situ measurement (Approximate time differences was 15 days) to tested out the performance of the new algorithm. As for the data that was selected for each of those years was the scene with the criteria of the lowest cloud cover and nearest to the time of in-situ measurement, scene chosen for use in this study are presented in Table 1.

Table 1. Selected scene of Landsat 8 OLI.

Year	Scene ID	Acquisition Date
2015	LC81220642015147LGN00	27 Mei 2015
2016	LC81220642016134LGN00	13 Mei 2016
2017	LC08_L1TP_122064_20170516_20170525_01_T1	16 Mei 2017

The selected scene then corrected radiometric and atmospheric to change the digital number (DN) into corrected reflectances values. According to Landsat 8 handbook provided by U.S. Geological Survey (2016), the correction method was performed.The atmospheric correction is done by performed Dark Pixel methods or Dark Object Subtraction. This atmospheric correction method assumes that Rrs(λ) values that are sensed by the satellite sensor are affected by the atmospheric condition (Budhiman *et al.* 2013; Vanderstraete *et al.* 2004; Green *et al.* 2000). Dark Object Subtraction methods use the assumption that minimum pixel values that appeared other than zero are assumed from the atmosphere. Then, all pixel on the scene has to be subtracted by all minimum values (Jaelani et al., 2015; Lubis et al., 2017).

2.2.3 Radiometric data

The radiometric data that were used in this research consist of surface radiance, $L_u(\lambda)$, sky radiance, $L_{sky}(\lambda)$, and downwelling irradiance, $E_d(\lambda)$. Three of them are then processed into remote sensing reflectances, $R_{rs}(\lambda)$, and also diffuse attenuation coefficient, $K_d(\lambda)$. The radiometric data were measured by using a Hyperspectral Spectroradiometer sensor from TriOS-RAMSES, which belongs to Remote Sensing Applications Center of National Institute of Aeronautics and Space of Indonesia (LAPAN), Jakarta, Indonesia. The data were recorded by a software called *Multi-Sensor Data Acquisition* (MSDA_XE ver. 8.9.2 2014-04-28), which was provided by TriOS GmbH and the data were radiometric calibrated by a constant that comes from the software. The TriOS-RAMSES sensors were calibrated by Remote Sensing Applications Center of LAPAN using white reference and dark reference panel provided by TriOS.

One of three sensors was an irradiance sensor (ACC-2-VIS), and the other two were radiance sensors (ARC-VIS) with 7° field-of-view. All sensors from TriOS-RAMSES work within the wavelength range of 320 nm to 950 nm and spectral sampling of 3.3 nm. We also conducted the validation between *remote sensing reflectances*, $R_{rs}(\lambda)$ from in-situ measurement with Landsat 8 OLI based *remote sensing reflectances*, $R_{rs}(\lambda)$. The illustration of TriOS-RAMSES sensors configuration is described as follows (Figure 2).

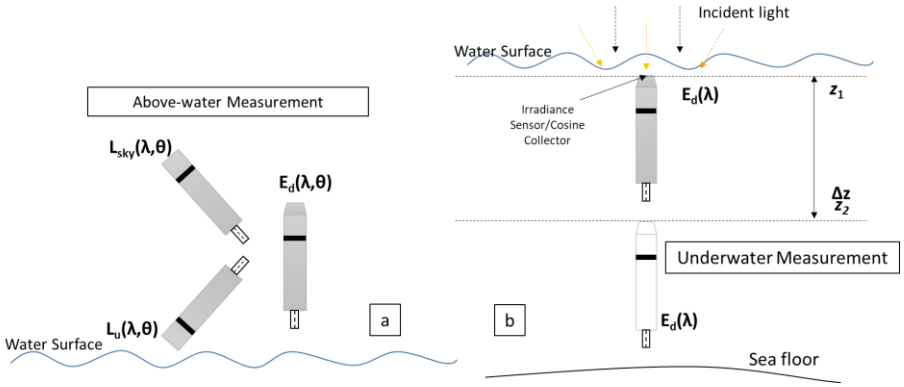

Fig. 2. Illustration of TriOS-RAMSES's sensors configuration during field measurement; (a) measurement of $R_{rs}(\lambda)$; (b) measurement of $E_d(\lambda)$ (Prasetyo et al., 2017).

The recording of the location coordinate was carried out using handheld GPS Garmin Montana 680 with the margin of error for the exact location within 3.65 m, concurrently with the recording of the atmospheric condition and radiometric measurement. The radiometric measurement itself was divided into two measurements, above-water measurement to derived reflectances by using all three sensors, and under-water measurement to derived diffuse attenuation $K_d(\lambda)$ from downwelling irradiance $E_d(\lambda)$. For reflectances, the cosine collector ($E_d(\lambda)$) was pointed upward for collecting the incident sky radiation. Meanwhile, a radiance sensor was pointed in the upward direction of 135° to measure the incident sky radiance $L_{sky}(\lambda)$. The second sensor was the radiance sensor, it was pointed in the downward direction of 45° to measure the total radiance, $L_u(\lambda)$, it configuration of three sensors in accordance by Mueller *et al.* (2003) (Figure 2(a)). Meanwhile, for diffuse attenuation from downwelling irradiance, the cosine collector was pointed out to 90° to zenith and measurement was done at two different depth $z_1 - z_2$, it was in accordance to Kirk (2011) (Figure 2(b)).

The radiometric data from MSDA_XE then extracted, it consists of downwelling irradiance $E_d(\lambda)$, sky radiance $L_{sky}(\lambda)$, and surface radiance $L_u(\lambda)$, then extracted to tab-delimited format for the next process. The $E_d(\lambda)$ then plotted for curve fitting with the exponential function from the $E_d(\lambda)$ itself. Values of $K_d(\lambda)$ can be calculated using the $E_d(\lambda)$ data on two different depth level from RAMSES

spectroradiometer by downward irradiance on hyperspectral wavelength centered on λ (Kirk, 2011) (Equation 1).

$$K_d(\lambda) = \frac{1}{z_2 - z_1} ln \frac{E_d(z_1,\lambda)}{E_d(z_2,\lambda)} \quad (1)$$

where, z_2-z_1 is the differences of depth level on each measurement (m), and E_d is the values of downwelling irradiance at depth z at wavelength λ. The K_d data at 490 nm then used in this research to derived $K_d(490)$ based on Landsat 8 OLI imagery data.

Remote Sensing Reflectances $R_{rs}(\lambda)$ is calculated from above water measurement, and it was a ratio between the *water-leaving radiance* ($L_w(\lambda)$) and *downwelling irradiance* ($E_d(\lambda)$) (Mobley 1999; Budhiman *et al.* 2012):

$$R_{rs}(\lambda) = \frac{L_w(\lambda)}{E_d(\lambda)} \quad (2)$$

Water-leaving radiance, $L_w(\lambda)$, was calculated from the measurement of *upwelling radiance,* $L_u(\lambda)$, on the surface, where the total radiance comes from the water surface then sensed by the sensor, which is consisted by water-leaving radiances and sky radiance that reflected by above water surface. The water-leaving radiance itself can be calculated using Equation 3 (Mueller et al., 2003),

$$L_w(\lambda) = L_u(\lambda) - \rho_{sky} . L_{sky}(\lambda) \quad (3)$$

where $L_u(\lambda)$ is the upwelling radiance measurement, that is all radiance that comes from the above water surface or by surface reflectances, $L_{sky}(\lambda)$ is from downwelling radiance measurement that comes from sky, $\rho_{sky}(\lambda)$ is coefficient from water-sky interaction that can be calculated using *Fresnel* equation (Budhiman et al., 2012).The remote sensing reflectance data then used to develop an empirical model to derive $K_d(490)$ based on Lee *et al.* (2005) and to simulate remote sensing reflectance data from Landsat 8 OLI to derive $K_d(490)$ values from developed empirical models.

2.3 Accuracy assessment

Several accuracy assessments were carried out to the new developed empirical algorithm of $K_d(490)$ against $K_d(490)$ from in-situ measurement to study about the algorithm performances. The mean absolute deviation (MAD), mean absolute percentage error (MAPE) and root-mean-square error (RMSE) were calculated to indicate the accuracy of the $K_d(490)$ models (Makridakis, 2000), the equation written below:

$$MAD = \frac{1}{n} \sum_{t=1}^{n} |X_t - F_t| \quad (4)$$

$$MAPE = \left(\frac{100\%}{n}\right) \sum_{t=1}^{n} \frac{|X_t - F_t|}{X_t} \quad (5)$$

$$RMSE = \sqrt{\frac{1}{n} \sum_{t=1}^{n} (X_t - F_t)^2} \quad (6)$$

where, X_t has measured values for *t*- sample, F_t was predicted values for *t*- sample and *n* was the number of samples. MAD showed the deviation of estimated $K_d(490)$ in m^{-1} (Equation 4), MAPE showed the percentage of error (Eq. 5), and RMSE showed the root mean square of error from estimated $K_d(490)$ (Equation 6).

3. Results and Discussion

3.1 $K_d(\lambda)$ Values Variability

The measurement of $K_d(\lambda)$ was conducted to assess the variability of optical properties on these three lagoonal area. According to Prasetyo *et al.* (2017) the results of measurement generally on each point that on the middle of Karang Lebar lagoon has the same patterns with Air island and Panggang island lagoon. On each location from the in-situ measurement of downwelling irradiance, showed that the averages values of $K_d(\lambda)$ on Karang Lebar lagoon was higher than Air Island lagoon and Panggang Island lagoon, it showed by the red line were dominantly over the other two lines on Figure 3 below for Karang Lebar lagoon.

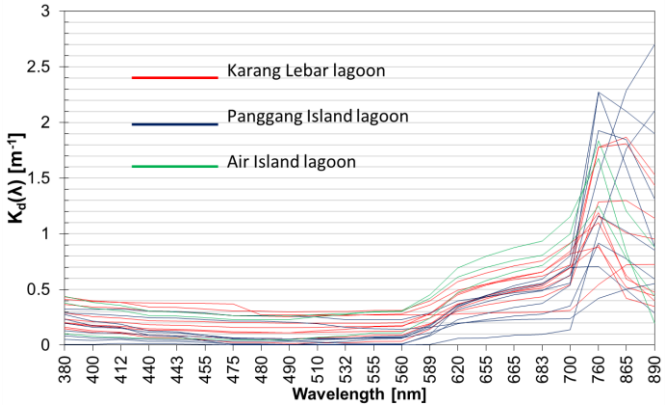

Fig. 3. Results of in-situ measurement diffuse attenuation on each respective area.

We also found that increasing of $K_d(\lambda)$ occurred in areas that were close to the coastal and in the middle of the lagoon area. This was probably due to the high concentration of chlorophyll-*a* and caused the absorption to increase (Prasetyo et al., 2017). It might be possibly caused by run off the organic and inorganic matters from Island, and high of waves caused the stirring of the bottom substrate that

dominantly consists of sand and other inorganic matters. Meanwhile, in the middle area of lagoons, $K_d(\lambda)$ was increased, $K_d(\lambda)$ on the outside lagoon to open water were decreased (Nababan et al., 2013). These circumstances were described by Brown *et al.* (2008) that open waters have optical properties that are influenced by organic matters like chlorophyll-a rather than inorganic matters like TSS.

Based on the in-situ measurement of Chlorophyll-*a,* Prasetyo *et al.* (2017) stated out that a high average of Chlorophyll-*a* values occurred on Panggang island lagoon and the lowest was on Air island. Based on TSS measurement, the high average of TSS values occurred on Karang Lebar lagoon and the lowest was on Panggang island lagoon. Measurement of $K_d(\lambda)$ values showed that light penetration on each sites was different. The lowest $K_d(\lambda)$ values showed the clearest water. $K_d(\lambda)$ was a part of AOP, so the composition of organic and inorganic matters in the water column has a great influence to penetrate the light on the water column (Kirk, 2011). Shallow waters have the characteristic that Chlorophyll-*a* concentration and TSS were high; it affects to absorption and scattering of light penetration through the water column (Saulquin et al., 2013). Wang *et al.* (2008) state that $K_d(\lambda)$ is influenced by the absorption coefficient from water molecules and the light field distribution on its water constituent. Prasetyo *et al.* (2017) stated out that on each respective area from in-situ measurement, $K_d(\lambda)$ value was dominantly affected by absorption of organic matters such as chlorophyll-*a* compared to scattered of inorganic matters such as suspended solids, those things was in line with Brown *et al.* (2008) statement.

Table 2. General forms of the new developed algorithms.

Green and NIR	NIR and Green
$K_d(490) = a * \left(\frac{R_{rs}(Green)}{R_{rs}(NIR)}\right) + b$	$K_d(490) = a * \left(\frac{R_{rs}(NIR)}{R_{rs}(Green)}\right) + b$
$K_d(490) = a * \ln\left(\frac{R_{rs}(Green)}{R_{rs}(NIR)}\right) + b$ (7)	$K_d(490) = a * \ln\left(\frac{R_{rs}(NIR)}{R_{rs}(Green)}\right) + b$ (8)

3.2 $K_d(490)$ algorithm for Landsat 8 OLI development

Several retrieval models for $K_d(490)$ have been developed for operational use (IOCCG 2000; IOCCG 2006), and there have been no universal models to retrieved $K_d(490)$ for shallow-coastal waters by using medium spatial imagery data. Previous models have been proposed earlier was to retrieve $K_d(490)$ over inland turbid waters (Zheng et al., 2016). Landsat 8 OLI data has the potential to map the value of $K_d(490)$ in regional waters in Indonesia. Landsat 8 OLI data could provide solutions to spatial data availability of $K_d(490)$ values in addition to Ocean Color data. In addition, only 4 pixels available for $K_d(490)$ data over our research location by using the KD2 algorithm on Ocean Color data daily and monthly. Thus, the development of the local algorithm of $K_d(490)$ is necessary to cover the small region of coastal shallow-water based on our result. In accordance with Zheng *et al.* (2016), for the purpose of determining the best band ratio, correlation analysis was carried out between $K_d(490)$ from in-situ measurement as the dependent variable against simulated Landsat 8 OLI bands as an independent variable that also from an in-situ measurement. We were using the same band combination as Zheng *et al.* (2016), between R_{rs}(Green) and R_{rs}(NIR), that band combination was used to developed $K_d(490)$ algorithm with the highest coefficient of determination among another different band ratio; also we tested out by two simple linear functions, i.e., linear and logarithmic. Our new algorithm general forms to estimate $K_d(490)$, as follows (Table 2), where, R_{rs}(Green) and R_{rs}(NIR) are the Green and Near Infrared band $R_{rs}(\lambda)$ values from Landsat 8 OLI after atmospheric correction, *a* and *b* were a constant from regression analysis. Zheng *et al.* (2016) stated out that thus band ratio algorithm for estimating various water types were usually done, ranging from chlorophyll-a, CDOM, TSM, and water transparency to $K_d(490)$ have been developed.

Regression analysis between the two band ratio showed that logarithmic function between simulated Landsat 8 OLI R_{rs}(Green)/R_{rs}(NIR) and in-situ data of $K_d(490)$ has the best R^2 same as the simulated Landsat 8 OLI R_{rs}(NIR)/R_{rs}(Green). The coefficient of determination is 0.8719. Our new algorithm by using logarithmic function performed well on Green and NIR band ratio, shown by the validation between estimated $K_d(490)$ data with $K_d(490)$ from in-situ measurement (Figure 4(a)). The MAD of the $K_d(490)$ model for the Landsat 8 OLI validation dataset (Green and NIR) was 0.0197 m^{-1}, the RMSE was 0.0013, and the MAPE was 6.5841 %. If we compared to the NIR and Green ratio, the validation showed that Green and NIR has a lower error (Figure 4(b)). The NIR and Green band ratio algorithm was also validated with $K_d(490)$ from in-situ measurement (Figure 4(c)), the MAD was 0.0198 m^{-1}, the RMSE was 0.0013 and the MAPE was 6.5966 % (Figure 4(d)). The NIR and Green band ratio has a slightly greater error than the previous band ratio. The comparison between in-situ $K_d(490)$ data with derived $K_d(490)$ from our new developed algorithm on both band ratio was acceptable. Figure 4(b), 4(d) showed that in-situ data and derived $K_d(490)$ were distributed along a 1:1 line; this indicates that the algorithm can perform well over coastal shallow-waters.

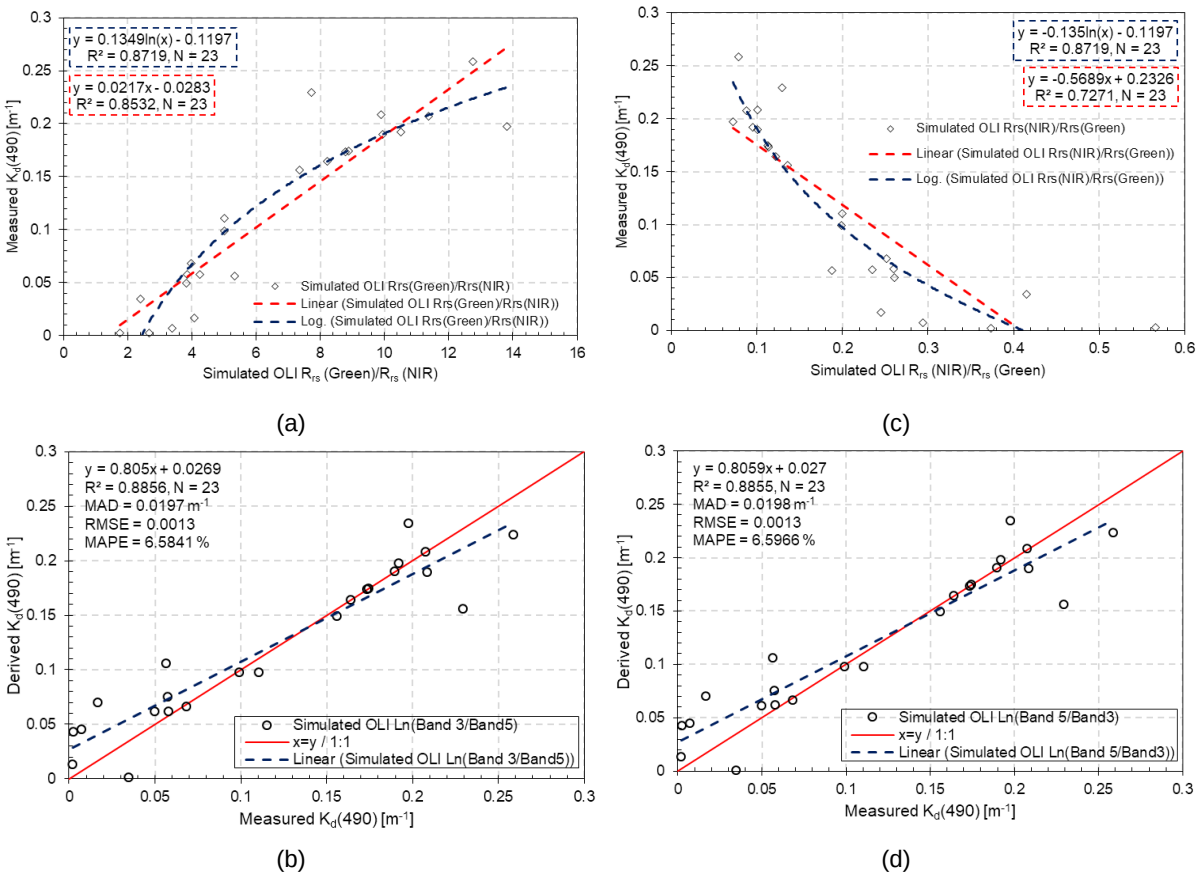

Fig. 4. Scatter plots of (a) $K_d(490)$ from in-situ measurement and Simulated Landsat 8 OLI R_{rs}(Green) and R_{rs}(NIR) band ratio, (b) $K_d(490)$ model validation between in-situ measurement and $K_d(490)$ that derived from Simulated Landsat 8 OLI, Green and NIR band ratio, (c) $K_d(490)$ from in-situ measurement and Simulated Landsat 8 OLI R_{rs}(NIR) and R_{rs}(Green) band ratio, (d) $K_d(490)$ model validation between in-situ measurement and $K_d(490)$ that derived from Simulated Landsat 8 OLI, NIR and Green band ratio.

3.3 Evaluation of Landsat 8 OLI derived $K_d(490)$ and algorithm accuracy

Ideally, times between in-situ measurement and the Landsat 8 OLI data should be concurrent within a limited period. But, we have difficulties in getting the clear Landsat 8 OLI data (without cloud or clear image). The evaluation for our new algorithm was conducted by using the image that was acquired at different times with the in-situ measurement (approximate 15 days of differences, the scene acquired at 13 Mei 2016). On our new algorithm that was using Simulated Landsat 8 OLI $R_{rs}(\lambda)$ should be performed well with atmospherically corrected Landsat 8 OLI. The accuracy of atmospheric corrected Landsat 8 OLI was evaluated through the comparison of the Landsat 8 OLI Based $R_{rs}(\lambda)$ and In-Situ measurement of Simulated Landsat 8 OLI band. We also compared between Landsat 8 OLI Based $K_d(490)$ and In-Situ measurement $K_d(490)$. According to Zheng *et al.* (2016), data from match-up points can be used to check the atmospheric correction for the $K_d(490)$ estimation model.

Comparisons between the $R_{rs}(\lambda)$ of Landsat 8 OLI band and In-Situ measurement of Simulated Landsat 8 OLI band on R_{rs}(Blue), R_{rs}(Green), R_{rs}(Red) and R_{rs}(NIR) showed that these values were in good. Figure 5 showed that the $R_{rs}(\lambda)$ of Landsat 8 OLI band and simulated $R_{rs}(\lambda)$ distributed along 1:1 line and Table 3 showed model assessment on each wavelength for these two comparisons.

Table 3. Model assessment between In-Situ $R_{rs}(\lambda)$ and the Landsat 8 OLI based $R_{rs}(\lambda)$ on each wavelength

Model Assessment	R_{rs}(Blue)	R_{rs}(Green)	R_{rs}(Red)	R_{rs}(NIR)
MAD	0.0138 sr^{-1}	0.0210 sr^{-1}	0.0223 sr^{-1}	0.0118 sr^{-1}
RMSE	0.0007	0.0011	0.0013	0.0006
MAPE	0.4283%	0.6710%	0.9991%	1.1400%

After the comparison between measured In-Situ $R_{rs}(\lambda)$ and the Landsat 8 OLI based $R_{rs}(\lambda)$, we also validate the Landsat 8 OLI based $K_d(490)$ with $K_d(490)$ data from in-situ measurement (Figure 6). The scatter plots were slightly distributed under the 1:1 line; this thing happens might due to the differences time between in-situ measurement and Landsat 8 OLI data acquisition. The MAD of Kd(490) was 0.0785 m-1, the RMSE was 0.0042 and the MAPE was 10.6430%. This was demonstrated that the new algorithm to retrieve $K_d(490)$ performed well. By using the new algorithm to retrieve $K_d(490)$ based on Landsat 8 OLI over a small region, this algorithm could be used to study temporal and spatial patterns on coastal shallow-waters such as Panggang Island lagoon and Karang Lebar lagoon.

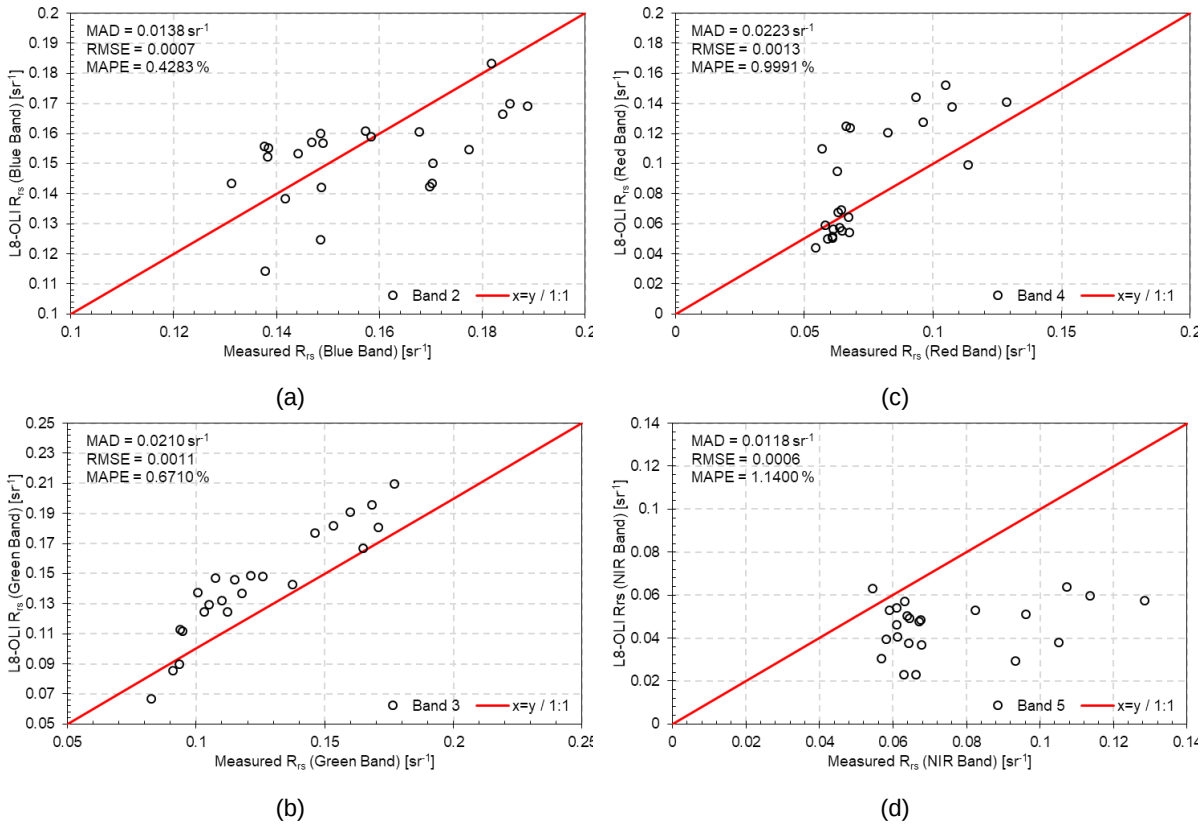

Fig. 5. Comparison of measured In-Situ $R_{rs}(\lambda)$ and the Landsat 8 OLI based $R_{rs}(\lambda)$ at (a) blue band, (b) green band, (c) red band, (d) NIR band after atmospheric correction.

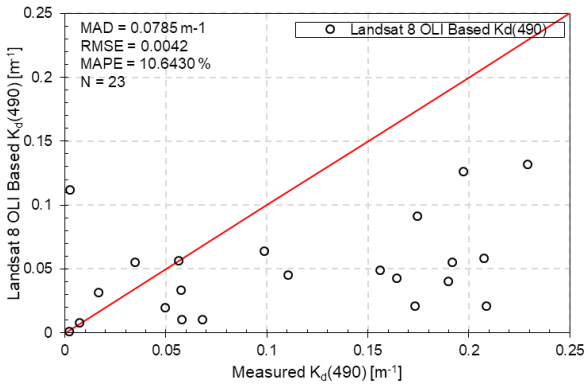

Fig. 6. Comparison Landsat 8 OLI based $K_d(490)$ with $K_d(490)$ data from in-situ measurement, the image was acquired at 13 Mei 2016.

3.4 Comparison between another $K_d(490)$ algorithm

The previously proposed algorithm to retrieve $K_d(490)$ from Landsat 8 OLI over inland turbid waters (Zheng et al., 2016) and another empirical algorithm of $K_d(490)$ (Lee et al., 2005) then used to compare the performances of our new proposed algorithm. Zheng *et al.* (2016) algorithm were using NIR and Green band ratio same as our new algorithm.

Meanwhile, Lee *et al.* (2005) empirical algorithm using $K_w(490)$ or pure water attenuation at 490 nm as input, and using the ratio of E_d and R_{rs} at 490 nm and 555 nm on their algorithm's that derived from $K_d(490)$ algorithm on Ocean Optics Protocols for Sattelite Ocean Color Sensor Validation (Mueller et al., 2003). These empirical models were used to describe the relationship between the $R_{rs}(\lambda)$ at the blue and green wavelength region with a simple regression to assess the correlation between the values of $K_d(490)$ with water-leaving radiance at blue wavelength region (λ = 443 nm) and green (λ = 555 nm), that empirical model is used to derive $K_d(490)$ from Sea-Viewing Wide Field-of-view (SeaWiFS) sensors (Austin and Petzold, 1981; Austin and Petzold, 1984; Morel and Maritorena, 2001; Smith and Baker, 1981; Mueller *et al.* 2003). $K_d(490)$ is assumed has correlation with pure water attenuation coefficient ($K_w(490)$ = 0,016 m^{-1}), the equation can be written as follows:

$$K_d(490) = K_w(490) + A\left(\frac{L_w(\lambda_1)}{L_w(\lambda_2)}\right)^B \quad (9)$$

where, *A* and *B* is constant, and $K_w(490)$ is attenuation coefficient for pure seawater. Then Mueller *et al.* (2003) stated that water-leaving radiances (L_w) at the blue and green wavelength region is suitable with the dataset provides by SeaWiFS is at 450 nm and 555 nm sequentially. Equation 9 can be rewritten as follows:

$$K_d(490) = K_w(490) + 0{,}15645\left(\frac{L_w(490)}{L_w(555)}\right)^{-1{,}5401} \quad (10)$$

Lee *et al.* (2005) also stated that remote sensing reflectances (R_{rs}) could be calculated between the ratio of water-leaving radiances with downwelling irradiance that measured just above the surface, with the E_d ratio is at $E_d(490)$ and $E_d(555)$. Note that $E_d(490)/E_d(555)$ results from field measurement only slightly around 1,3 occurred on this research on various sun angle, so the E_d ratio is set to constant, then the Equation 10 can be rewritten as follows:

$$K_d(490)_{derived} = K_w(490) + 0{,}15645\left(1{,}3\frac{R_{rs}(490)}{R_{rs}(555)}\right)^{-1{,}5401} \quad (11)$$

equation above (Equation 11) on this research can be used to calculate $K_d(490)$ values derived from R_{rs} that measured from above water; then the results is can be used to see the difference between derived $K_d(490)$ and measured $K_d(490)$.

Zheng *et al.* (2016) algorithm for Landsat 8 OLI derived underestimate values and did not distribute along 1:1 line when it applied by our datasets from In-Situ measurement (Figure 7). It has a greater error than the new algorithm that we proposed, showed by MAD was 0,0957 m^{-1}, RMSES was 0,0048 and MAPE was 13,7442%. Also, Lee *et al.* (2005) algorithm derived an overestimate and has greater error, showed by the scatter plots that distributed dominantly to derived $K_d(490)$ (Figure 7(b)). Meanwhile, Zheng *et al.* (2016) was algorithm for inland turbid waters that has different optical characteristics, and dominantly affected by scattering caused by suspended solids. Statistically on Zheng algorithm has greater linear relationship showed by coefficient of determination 0,8719 greater than Lee algorithm 0,7062. It might happens caused by different approach of wavelength that were used on their algorithm. Lee algorithm were used ratio of $R_{rs}(490)/R_{rs}(555)$ to calculate the attenuation change caused by absorption from water molecules and chlorophyll-a concentration, it means Lee algorithm has similarity approximate values of $K_d(490)$ showed by the scatter plots that slightly distributed around 1:1 line compared to Zheng algorithm. On the previous research also stated that waters around Panggang Island lagoon dominant affected by absorption caused by chlorophyll-*a* (Prasetyo et al., 2017).

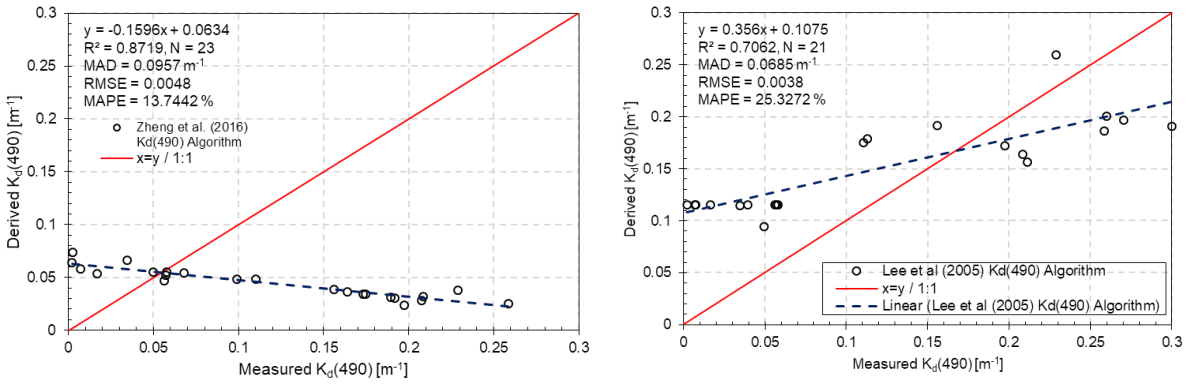

(a) (b)

Fig. 7. Comparison between another empirical $K_d(490)$ algorithm performance with $K_d(490)$ from In-Situ measurement, (a) Zheng *et al.* (2016) algorithm, (b) Lee *et al.* (2005) algorithm.

Table 4 below showed the performances and algorithm form of $K_d(490)$ compared to another empirical algorithm were proposed earlier. This research proposes the two-band ratio algorithm which can be used on Landsat 8 OLI data, the ratio between the Green (533 nm - 590 nm) and NIR (851 nm - 879 nm) bands. The performance of the algorithm that has been developed based on the results of the accuracy assessment is 0.0197 m^{-1} and 0.0198 m^{-1} of the mean absolute deviation, and 6.5841% and 6.5966% of the mean absolute percentage error then it has a root mean square error of 0.0013 for both band ratios.

Table 4. Comparison of $K_d(490)$ algorithm performances.

Model by	$K_d(490)$ Algorithm	R^2	MAD (m^{-1})	MAPE (%)	RMSE
Lee *et al.* (2005)	$K_d(490) = 0.016 + 0.15645\left(\frac{E_d(490)}{E_d(555)}\frac{R_{rs}(490)}{R_{rs}(555)}\right)^{-1.5401}$	0.7062	0.0685	25.3272	0.0038
Zheng *et al.* (2016)	$K_d(490)_{\text{L8-OLI}} = 2.468 * \ln\left(\frac{R_{rs}(NIR)}{R_{rs}(Green)}\right) + 8.81$	0.8719	0.0957	13.7442	0.0048
This research	$K_d(490)_{\text{L8-OLI}} = 0.1349 * \ln\left(\frac{R_{rs}(Green)}{R_{rs}(NIR)}\right) - 0.1197$	0.8856	0.0197	6.5841	0.0013
	$K_d(490)_{\text{L8-OLI}} = -0.135 * \ln\left(\frac{R_{rs}(NIR)}{R_{rs}(Green)}\right) - 0.1197$	0.8855	0.0198	6.5966	0.0013

The comparison between this research algorithm performance and other algorithms (Lee et al., 2005); (Zheng et al., 2016) then plotted to line based on sampling station (Figure 8). we can conclude that our new algorithm of Kd(490) has approximate values near to Kd(490) from In-Situ measurement, showed by yellow and red lines that have the same patterns from In-Situ data (blue line). Also, we agreed that the previously developed algorithm (Zheng et al. 2016) to retrieve $K_d(490)$ by using our datasets was underestimate showed by the purple line, and it also did not have the same pattern.

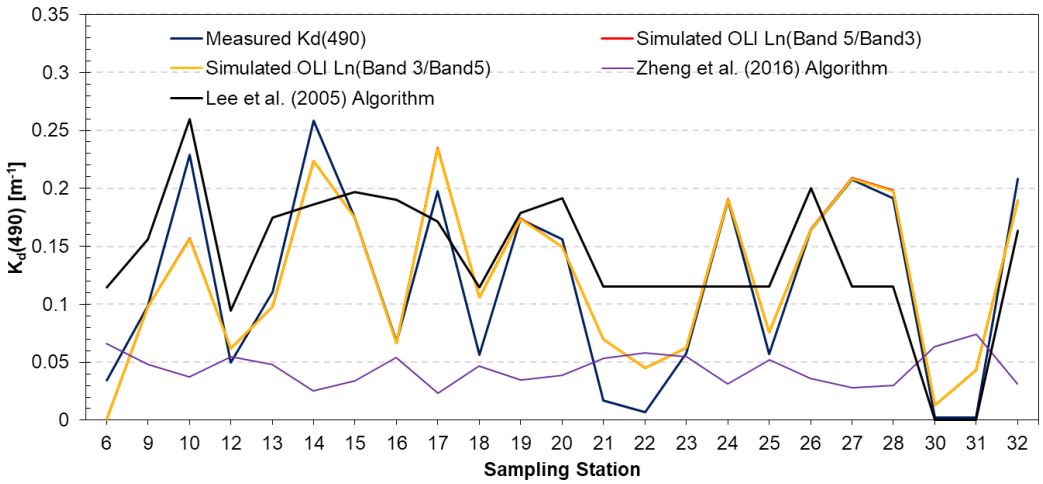

Fig. 8. Comparison of approximate values of $K_d(490)$ for each algorithm proposed, the thick blue line was from In-Situ measurement, yellow and red line were our new developed algorithm, the purple line was Zheng *et al.* (2016) algorithm, and black line was Lee *et al.* (2005).

3.5 Temporal and spatial patterns of $K_d(490)$

Spatial maps of $K_d(490)$ derived Landsat 8 OLI in waters around Panggang Island lagoon, Karang Lebar lagoon, and Air Island lagoon, using our new algorithm are shown in Figure 9. With the selected scenes from different years (2015, 2016, and 2017), we can study the patterns of $K_d(490)$ over the small regions such as our research locations that can not be derived from operational KD2 Algorithm of Ocean Color data.

As can be seen from Figure 9 and Figure 10 above that patterns of Kd(490) values in 2015 are lower than in 2016 and 2017. In 2016, averages values of $K_d(490)$ around Karang Lebar lagoon were decreased despite that color are red that indicate high values of pixels. But in 2016, the red color for pixes of $K_d(490)$ values has lower values than in 2015 and 2017. We can conclude that $K_d(490)$ around Karang Lebar lagoon had been decreased on 2016 and increased again in 2017, that also patterns recurrent on another lagoons.

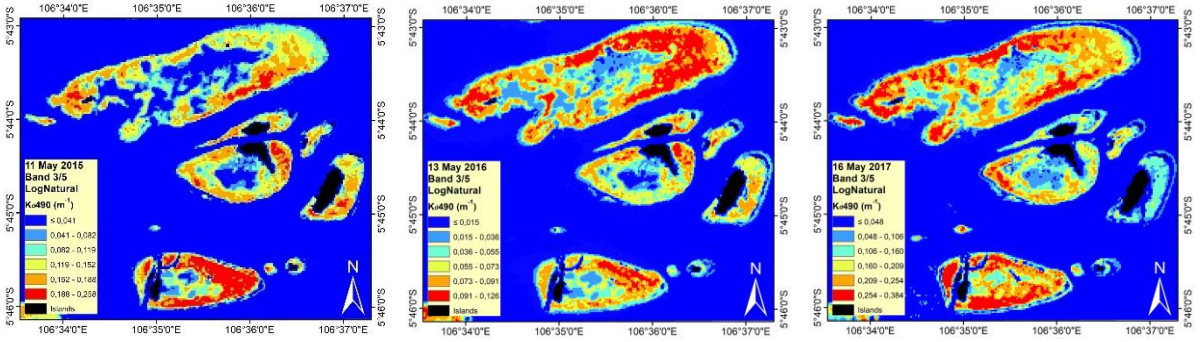

(a) (b) (c)

$$\text{Algorithm form: } K_d(490)_{L8-OLI} = 0.1349 * \ln\left(\frac{R_{rs}(Green)}{R_{rs}(NIR)}\right) - 0.1197$$

Figure 9. Spatial distributions of $K_d(490)$ by using Landsat 8 OLI based band ratio $R_{rs}(Green)$ and $R_{rs}(NIR)$ of new developed algorithm, images acquired at (a) 11 May 2015, (b) 13 May 2016 and (c) 16 May 2017.

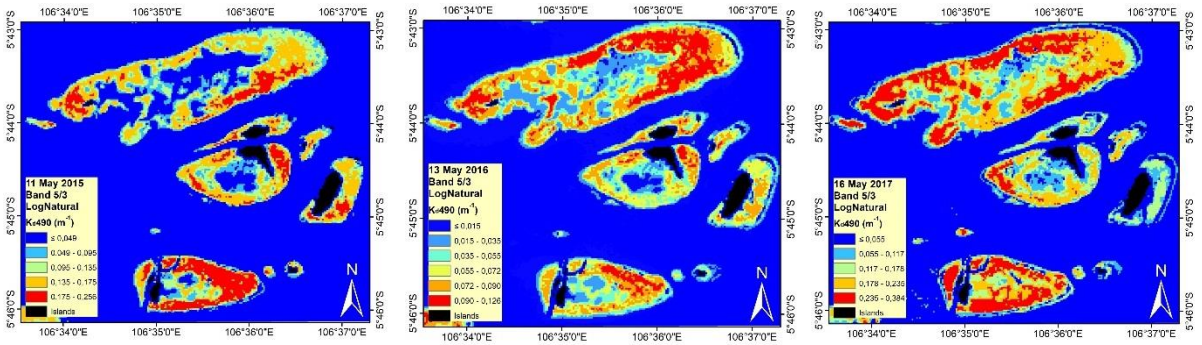

(a) (b) (c)

$$\text{Algorithm form: } K_d(490)_{L8-OLI} = -0.135 * \ln\left(\frac{R_{rs}(NIR)}{R_{rs}(Green)}\right) - 0.1197$$

Figure 10. Spatial distributions of $K_d(490)$ by using Landsat 8 OLI based band ratio $R_{rs}(NIR)$ and $R_{rs}(Green)$ of new developed algorithm, images acquired at (a) 11 May 2015, (b) 13 May 2016 and (c) 16 May 2017.

4. Conclusion

The newly developed $K_d(490)$ of Landsat 8 OLI can perform well among other empirical $K_d(490)$ algorithms and applicable at a small region of shallow-waters in Panggang Island lagoon and Karang Lebar lagoon. The best newly developed algorithm to derive $K_d(490)$ using Landsat 8 OLI was empirically built by the ratio of R_{rs} at Green and Near-Infrared band; it has good performances and showed a lower error than among others empirical algorithm proposed in the earlier study. The approximate values of the new $K_d(490)$ empirical algorithm have the same pattern as the in-situ measurement, and it has a lower error of validation among other empirical algorithms. The variability of $K_d(490)$ values based on the new algorithm on shallow-waters around Panggang Island from temporal data of Landsat 8 OLI imagery decreased in 2016, as shown in Figure 9 and Figure 10, and it increased in 2017.

5. References

Arief, M., 2017. Development of Dissolved Oxygen Concentration Extraction Model Using Landsat Data Case Study: Ringgung Coastal Waters. Int. J. Remote Sens. Earth Sci. 12, 1. https://doi.org/10.30536/j.ijreses.2015.v12.a2667

Austin, R.W., Petzold, T.J., 1984. Spectral Dependence Of The Diffuse Attenuation Coefficient Of Light In Ocean Waters. Ocean Opt. VII 0489, 168. https://doi.org/10.1117/12.943302

Austin, R.W., Petzold, T.J., 1981. The determination of the diffuse attenuation coefficient of sea water using the Coastal Zone Color Scanner. Oceanogr. from Sp. 239–256. https://doi.org/10.1017/CBO9781107415324.004

Brown, C.A., Huot, Y., Werdell, P.J., Gentili, B., Claustre, H., 2008. The origin and global distribution of second order variability in satellite ocean color and its potential applications to algorithm development. Remote Sens. Environ. 112, 4186–4203. https://doi.org/10.1016/j.rse.2008.06.008

Budhiman, S., Suhyb Salama, M., Vekerdy, Z., Verhoef, W., 2012. Deriving optical properties of Mahakam Delta coastal waters, Indonesia using in situ measurements and ocean color model inversion. ISPRS J. Photogramm. Remote Sens. 68, 157–169. https://doi.org/10.1016/j.isprsjprs.2012.01.008

Budhiman, S., Winarso, G., Asriningrum, W., 2013. Pengaruh Pengambilan Training Sample Substrat Dasar Berbeda pada Koreksi Kolom Air Menggunakan Data Penginderaan Jauh. Penginderaan Jauh 10, 83–92.

Green, E.P., Clark, C.D., Edwards, A.J., 2000. Image classification and habitat mapping. Remote Sens. Handb. Trop. Coast. Manag. 141–154.

Hendiarti, S.N., M.C.G, F., Andrastuti, A., Silaiman, A., 2006. Riset dan Teknologi Pemantauan Dinamika Laut Indonesia. Satelit Oseanografi 69.

IOCCG, 2006. IOCCG Report Number 05: Reports of the International Ocean-Colour Coordinating Group Remote Sensing of Inherent Optical Properties : Fundamentals, Tests of Algorithms, and Applications, IOCCG Report 5. https://doi.org/10.1006/jmbi.1998.2073

IOCCG, 2000. Reports of the International Ocean-Colour Coordinating Group Remote Sensing of Ocean Colour in Coastal , and Other Optically-Complex , Waters, Reports and Monographs of the International OceanColour Coordinating Group.

Jaelani, L.M., Setiawan, F., Wibowo, H., Apip, 2015. Pemetaan Distribusi Spasial Konsentrasi Klorofil-A dengan Landsat 8 di Danau Matano dan Danau Towuti , Sulawesi Selatan. Pros. Pertem. Ilm. Tah. XX 456–463. https://doi.org/10.13140/RG.2.1.4278.6000

Jerlov, N.G., 1976. Marine optics. Elsevier.

Kirk, J.T.O., 2011. Light and photosynthesis in aquatic ecosystems, third edition, Light and Photosynthesis in Aquatic Ecosystems, third edition. https://doi.org/10.1017/CBO9781139168212

Lee, Z.P., Darecki, M., Carder, K.L., Davis, C.O., Stramski, D., Rhea, W.J., 2005. Diffuse attenuation coefficient of downwelling irradiance: An evaluation of remote sensing methods. J. Geophys. Res. C Ocean. 110, 1–9. https://doi.org/10.1029/2004JC002573.

Lubis, M. Z., Taki, H. M., Anurogo, W., Pamungkas, D. S., Wicaksono, P., & Aprilliyanti, T. (2017, December). Mapping the distribution of potential land drought in Batam Island using the integration of remote sensing and geographic information systems (GIS). In IOP Conference Series: Earth and Environmental Science (Vol. 98, No. 1, p. 012012). IOP Publishing.

Lymburner, L., Botha, E., Hestir, E., Anstee, J., Sagar, S., Dekker, A., Malthus, T., 2016. Landsat 8: Providing continuity and increased precision for measuring multi-decadal time series of total suspended matter. Remote Sens. Environ. 185, 108–118. https://doi.org/10.1016/j.rse.2016.04.011

Makridakis, S., 2000. The M3-Competition : results , conclusions and implications 16, 451–476.

Mobley, C.D., 1999. Estimation of the remote-sensing reflectance from above-surface measurements. Appl. Opt. 38, 7442. https://doi.org/10.1364/AO.38.007442

Morel, A., Maritorena, S., 2001. Bio-optical properties of oceanic waters: A reappraisal. J. Geophys. Res. Ocean. 106, 7163–7180. https://doi.org/10.1029/2000JC000319

Mueller, J.L., Bidigare, R.R., Trees, C., Balch, W.M., Dore, J., Drapeau, D.T., Karl, D.M., Van Heukelem, L., Perl, J., 2003. Ocean optics protocols for satellite ocean color sensor validation, Revision 5, Volume V: Biogeochemical and bio-optical measurements and data analysis protocols. Ocean Color web page V, 36.

Nababan, B., Louhenapessy, V.S.A., Arhatin, R.E., 2013. DOWNWELLING DIFFUSE ATTENUATION COEFFICIENTS FROM IN SITU MEASUREMENTS OF DIFFERENT WATER TYPES. Int. J. Remote Sens. Earth Sci. 10.

Pahlevan, N., Schott, J.R., 2013. Leveraging EO-1 to evaluate capability of new generation of

landsat sensors for coastal/inland water studies. IEEE J. Sel. Top. Appl. Earth Obs. Remote Sens. 6, 360–374. https://doi.org/10.1109/JSTARS.2012.2235174

Parwati, E., Purwanto, A.D., 2017. Time Series Analysis of Total Suspended Solid (Tss) Using Landsat Data in Berau Coastal Area, Indonesia. Int. J. Remote Sens. Earth Sci. 14, 61. https://doi.org/10.30536/j.ijreses.2017.v14.a2676

Prasetyo, B.A., Siregar, V.P., Agus, S.B., Asriningrum, W., 2018. PENGUKURAN KOEFISIEN DIFFUSE ATENUASI (Kd) DI PERAIRAN DANGKAL SEKITAR KARANG LEBAR, KEPULAUAN SERIBU, DKI JAKARTA. J. Teknol. Perikan. dan Kelaut. 8, 127. https://doi.org/10.24319/jtpk.8.127-138

Prasetyo, B.A., Siregar, V.P., Agus, S.B., Asriningrum, W., 2017. IN-SITU MEASUREMENT OF DIFFUSE ATTENUATION COEFFICIENT AND ITS RELATIONSHIP WITH WATER CONSTITUENT AND DEPTH ESTIMATION OF SHALLOW WATERS BY REMOTE SENSING TECHNIQUE. Int. J. Remote Sens. Earth Sci. 14, 47. https://doi.org/10.30536/j.ijreses.2017.v14.a2682

Salama, M.S., Verhoef, W., 2015. Two-stream remote sensing model for water quality mapping: 2SeaColor. Remote Sens. Environ. 157, 111–122. https://doi.org/10.1016/j.rse.2014.07.022

Saulquin, B., Hamdi, A., Gohin, F., Populus, J., Mangin, A., d'Andon, O.F., 2013. Estimation of the diffuse attenuation coefficient KdPAR using MERIS and application to seabed habitat mapping. Remote Sens. Environ. 128, 224–233. https://doi.org/10.1016/j.rse.2012.10.002

Smith, R.C., Baker, K.S., 1981. Optical properties of the clearest natural waters (200--800 nm). Appl. Opt. 20, 177–184.

U.S. Geological Survey, 2016. Landsat 8 Data Users Handbook. Nasa 8, 97.

Vanderstraete, T., Goossens, R., GHABOUR, T., 2004. Coral reef bottom-type mapping in the Red Sea (Hurghada, Egypt) based on remote sensing. EARSeL eProceedings 3 (2), 191–207.

Wang, G., Cao, W., Yang, D., Xu, D., 2008. Variation in downwelling diffuse attenuation coefficient in the northern South China Sea. Chinese J. Oceanol. Limnol. 26, 323–333. https://doi.org/10.1007/s00343-008-0323-x

Wang, M., Son, S.H., Harding, L.W., 2009. Retrieval of diffuse attenuation coefficient in the Chesapeake Bay and turbid ocean regions for satellite ocean color applications. J. Geophys. Res. Ocean. 114, 20482–20493. https://doi.org/10.1029/2009JC005286

Zheng, Z., Ren, J., Li, Y., Huang, C., Liu, G., Du, C., Lyu, H., 2016. Remote sensing of diffuse attenuation coefficient patterns from Landsat 8 OLI imagery of turbid inland waters: A case study of Dongting Lake. Sci. Total Environ. 573, 39–54. https://doi.org/10.1016/j.scitotenv.2016.08.019